Author Manuscript

Author Manuscript

Author Manuscript

Author Manuscript

HHS Public Access

Author manuscript

ASAIO J. Author manuscript; available in PMC 2018 March 01.

Published in final edited form as:

ASAIO J. 2017 ; 63(2): 198–206. doi:10.1097/MAT.0000000000000460.

Scaling the low-shear pulsatile TORVAD for pediatric heart failure

Jeffrey R. Gohean[*], **Erik R. Larson**[*], **Brian H. Hsi**[†], **Mark Kurusz**[*], **Richard W. Smalling**[†], and **Raul G. Longoria**[‡]

[*]Windmill Cardiovascular Systems, Austin, Texas

[†]Division of Cardiovascular Medicine, University of Texas Medical School at Houston and The Memorial Hermann Heart and Vascular Institute, Houston, Texas

[‡]Department of Mechanical Engineering, University of Texas at Austin, Austin, Texas

Abstract

This article provides an overview of the design challenges associated with scaling the low-shear pulsatile TORVAD ventricular assist device (VAD) for treating pediatric heart failure. A cardiovascular system model was used to determine that a 15 ml stroke volume device with a maximum flow rate of 4 L/min can provide full support to pediatric patients with body surface areas between 0.6 to 1.5 m^2. Low shear stress in the blood is preserved as the device is scaled down and remains at least two orders of magnitude less than continuous flow VADs. A new magnetic linkage coupling the rotor and piston has been optimized using a finite element model (FEM) resulting in increased heat transfer to the blood while reducing the overall size of TORVAD. Motor FEM has also been used to reduce motor size and improve motor efficiency and heat transfer. FEM analysis predicts no more than 1°C temperature rise on any blood or tissue contacting surface of the device. The iterative computational approach established provides a methodology for developing a TORVAD platform technology with various device sizes for supporting the circulation of infants to adults.

Introduction

The etiology of heart failure (HF) in children is primarily due to the effects of congenital cardiac defects or acquired cardiomyopathy, and they account for up to 14,000 hospitalizations per year in the United States (1, 2). While many of these children undergo corrective or palliative cardiac surgical procedures, heart transplantation often remains the only treatment for decompensating heart failure. Unfortunately, the availability of donor hearts is limited and hundreds of children die each year while awaiting transplantation (1, 3). Ventricular assist devices are pumps that augment cardiac output and have been used successfully to save lives in the pediatric patient population. However, challenges with

Address for correspondence: Jeffrey R. Gohean, Windmill Cardiovascular Systems, Inc., 7801 N. Lamar Blvd, Ste E212, Austin, TX 78752 U.S.A., Tel # 512-419-9947, Fax # 512-419-9597, jgohean@windmillcvs.com.

Disclosures: Drs. Longoria and Smalling have an equity interest in Windmill Cardiovascular Systems, Inc. The authors have no other conflicts of interest to report.

Author Manuscript Author Manuscript Author Manuscript Author Manuscript

VADs in pediatrics remain because their use is associated with a high incidence of bleeding and neurological dysfunction (4, 5), and there has been limited clinical application due to sizing requirements in smaller age groups. All intrathoracic pediatric VADs currently under development are continuous flow (CF), impeller-based designs that are likely to result in similar complications as seen in adults, particularly those associated with the induced high shear and lack of pulsatility. This paper describes the design of an alternative small, implantable, low-shear pulsatile VAD based on a two-piston technology that can maintain adequate circulatory support with reduced risk of complications.

Miniaturization of VADs is necessary to achieve intracorporeal placement in pediatrics, and this goal has driven the development of small, implantable CF devices over the last decade, such as the ReliantHeart HeartAssist 5 Child® and the Infant Jarvik 2015. Intracorporeal placement of pediatric VADs could improve mobility and allow patients to be discharged from the hospital. Continuous flow pumps generate flow using an impeller that operates at speeds of several thousand revolutions per minute (rpm). A significant trade-off in miniaturization of CF pumps is the need for higher rotational speeds to achieve adequate flow that can further compound increased shear stress in the blood, which is already several orders of magnitude above normal physiological conditions. These high-shear conditions cause damage and depletion of important blood constituents, such as high-molecular-weight (HMW) von Willebrand Factor (vWF), which is especially sensitive to shear. Most CF VAD patients develop acquired von Willebrand Disease, a coagulopathy that hinders the ability of platelets to adhere to bleeding sites, possibly resulting in serious bleeding complications as reported in 40% of CF VAD patients (6). Elevated shear stress also causes platelet activation and aggregation that can lead to increased risk of pump thrombosis and embolic stroke (7–9). The antiplatelet and anticoagulation therapy administered to prevent such events often leads to secondary complications such as heparin-induced thrombocytopenia and gastrointestinal (GI) bleeding (10–12). White blood cell function also can be inhibited by elevated shear, increasing the risk of infections in CF VAD recipients (13, 14). Hematological and bleeding outcomes for pediatric CF devices in development are not known, but it stands to reason that complications evident in adult patients with CF pumps will also impact pediatric patients. The two-piston pumping paradigm inherent to the VAD design to be described in the following section can meet the circulatory support needs of both adult and pediatric HF patients while maintaining low-shear.

System Description

Windmill Cardiovascular Systems, Inc. has developed a new two-piston pumping paradigm to deliver synchronous, pulsatile flow with low shear called TORVAD (TORoidal VAD). The TORVAD operates differently than previous pulsatile devices and is smaller, which allows it to be implanted in the pre- or intra-peritoneal position. The system normally operates synchronously with the cardiac cycle by delivering a 30 ml ejection in early diastole, but can automatically adapt to pump asynchronously from 1 to 8 L/min to deliver full support.

The pump consists of a toroidal-shaped pumping chamber with inlet and outlet ports and two pistons independently controlled to move within the chamber lumen as illustrated in the schematic in Figure 1. Each piston is comprised of hermetically-sealed, rare earth magnets

Author Manuscript Author Manuscript Author Manuscript Author Manuscript

that interact with a magnetic coupling that rotates along the outer surface of the pumping chamber attached to the rotor of a position-controlled motor. Pumping is achieved by driving one piston within the toroidal pumping chamber while the other piston is momentarily held between the inlet and outlet ports, thereby maintaining unidirectional flow. At the completion of each stroke, the pistons exchange functional roles, achieving positive-displacement, pulsatile flow without use of conventional valves. Using a standard pacemaker sensing lead and electrocardiogram (ECG) amplifier, the VAD controller senses and can synchronize pump ejections with the native heart rhythm in any desired manner.

Low shear is enabled by the combination of low pump speed (mean rpm equal to heart rate) and a predetermined fixed gap between the piston and torus walls. A fixed gap (approximately 0.003″ in the current configuration) is achieved by using small ceramic hydrodynamic bearings. Dynamic start-stop bench-top experiments have shown that this bearing design can achieve a wear life in excess of 50 years, which is well beyond the expected life of the device. By maintaining a fixed gap between the piston and torus walls, shear is minimized to a level that is orders of magnitude lower than shear induced by CF pump impellers. There are numerous implications of substantially lower shear and reduced blood trauma compared to currently available devices. *In vitro* and *in vivo* testing has demonstrated this design results in very low hemolysis and does not deplete HMW vWF (15, 16). Consequently, there is potential to reduce the risk of bleeding. Other potential benefits of low shear pumping include decreased hemolysis, decreased platelet activation with associated pump thrombosis and embolic stroke, and preservation of white blood cell function that could lead to fewer infections. These benefits may be especially important for pediatric patients, who have greater adverse event rates with use of VADs compared to adult patients (17).

The primary synchronous operation mode of the TORVAD is an early diastolic counterpulse (18). By operating the pump in this mode, it briefly ceases to pump blood in systole, allowing the ventricle to eject normally through the aortic valve. This preservation of physiological function is in contrast to the manner whereby CF pumps reduce or eliminate aortic valve flow, which can lead to valve cusp fusion, thrombus formation, and a disruption of the Frank-Starling mechanism for cardiac output regulation. By preserving native aortic flow during TORVAD support, patency of the native aortic valve is maintained and the auto-regulatory aspect of the heart (Frank-Starling's Law) is preserved, thereby restoring the physiologic preload and afterload sensitivity of the cardiovascular system.

The dual-piston actuation mechanism of the TORVAD enables the measurement of the differential pressure across the pump using sensed motor currents(19). The TORVAD is a positive displacement device, so pressure on the pistons is proportional to the torque on the coupled motors. Motor torque and motor current are also proportional, providing a linear relationship between motor current and differential pressure. From this measurement, aortic blood pressure can be estimated, and it may be possible to infer left ventricular contractility (dP/dt) and systemic vascular resistance, which could be used to adjust pump operation should more or less flow be needed. The TORVAD has also been programmed to detect arrhythmias such as ventricular fibrillation and can automatically transition from

Author Manuscript Author Manuscript Author Manuscript Author Manuscript

synchronous mode to other pumping modes, such as a fixed flow rate up to 8 L/min, based on real-time cardiac monitoring.

Design for Pediatric Applications

Scaling the TORVAD for a pediatric patient requires a multi-objective optimization rather than a simple geometric scaling of system components of the device because key design parameters such as motor torque and efficiency and magnetic coupling forces do not scale linearly with size. Therefore, computational analysis involving multidisciplinary modeling tools must be used to optimize the device for different patient sizes while constraining those features to ensure low levels of blood shear stress are maintained.

The first step in sizing the device is to determine the pumping requirements such as the stroke volume, maximum flow rate, and expected operating pressures. Once those parameters are determined, a suite of software tools is used to design and develop key system components: the pump geometry and housing, motor/piston magnetic coupling, heat transfer pathways, and motors. Geometries and performance results from these analyses are interdependent, requiring an iterative process to arrive at an optimal solution.

By establishing the design methodology outlined above, the TORVAD's two-piston pumping technology can be adapted to different patient sizes, providing a platform for producing a variety of pump sizes from pediatric to a total artificial heart. The goal of this paper is to provide an overview for this methodology as it relates to the miniaturization of the device for children with a body surface area (BSA) between 0.6 and 1.5 m^2.

Design Results

Low Shear Preserved in Scaling

The majority of flow in the TORVAD (99.7% by blood volume) consists of the stroke volume through the toroidal pumping chamber. The torus hydraulic diameter is similar to the diameter of the aorta, so the bulk flow through torus has similar velocity and shear profiles as the flow through the aorta and major arterial vessels. The maximum shear stress in the TORVAD occurs not in the bulk flow, but in the leakage flow in the small annular gap between the rotating piston and the torus wall, which accounts for only 0.3% of the blood volume in the pump. In the annular gap, the Reynolds number is low ($Re \ll 100$) and the gap entrance length is short (<1% annular gap length), so the shear stress (τ) can be estimated analytically using the Couette-Poiseuille reduction of the Navier-Stokes equations (20).

$$\tau = \frac{1}{2}\frac{\mathrm{dP}}{\mathrm{dx}}(2\mathrm{y}-\mathrm{h}) + \frac{\mu\omega R}{\mathrm{h}}$$

Shear stress is a function of the pressure drop across the piston (dP/dx), gap height (h), blood viscosity (μ), rotational speed (ω), and piston radius (R) across the gap from the torus wall (y = 0) to the piston wall (y = h). Shear stress can be integrated to find the average shear stress,

Author Manuscript Author Manuscript Author Manuscript Author Manuscript

$$\tau_{avg}=\frac{1}{h}\int_0^h\left|\frac{1}{2}\frac{dp}{dx}(2y-h)+\frac{\mu\omega R}{h}\right|dy$$

and the maximum wall shear stress, which occurs at the piston wall (y = h), can be determined,

$$\tau_{max}=\frac{h}{2}\frac{dp}{dx}+\frac{\mu\omega R}{h}$$

For an adult TORVAD design with flow rate at 5 L/min and a differential pressure of 70 mmHg, the average shear in the gap is approximately 10 Pa, and the maximum does not exceed 50 Pa. This is two orders of magnitude lower than CF devices such as the Thoratec HeartMate II® (HMII) and HeartWare HVAD® that have maximum wall shear stresses above 2000 Pa at the same flow and pressure conditions (21).

Thamsen et al used computational fluid dynamic simulations to model the flow in the HMII and HVAD pumps to understand the blood damage potential of CF devices (21, 22). They calculated the volume of blood above approximate thresholds for vWF unfolding (9 Pa), platelet activation (50 Pa), and hemolysis (150 Pa) as a way of quantifying the damage potential of a device. No shear in the TORVAD exceeds 50 Pa, and only a small volume in the annular gap exceeds 9 Pa. The blood volume above 9 Pa has been plotted in Figure 2 along with the reproduced values found by Thamsen et al to provide a comparison.

Device scaling, particularly with CF devices, often comes with the cost of increased shear since rotational speed and fluid velocity requirements increase due to decreased size. In contrast, the TORVAD can scale while maintaining or even decreasing levels of fluid shear stress because the pressure, rotational speeds, and gaps remain the same for any stroke volume, but the velocity of the piston decreases as the radius of the device decreases, leading to an even further reduction in shear compared to the adult device.

Cardiovascular Model

TORVAD stroke volume and maximum flow rate requirements are determined using a lumped parameter model of the cardiovascular system to simulate hemodynamics with pulsatile synchronous support provided by the TORVAD. This model has been validated with *in vivo* data (23, 24). The inputs to the model are patient size and HF severity, for which the stroke volume and synchronous operation of the TORVAD can be optimized. This model has been previously used to determine the stroke volume and synchronous operation timing for an adult in end-stage HF (30 mL with an early diastolic synchronous counterpulse) (18). For the purposes of this design, the model has been adapted for pediatric HF by changing model parameters (e.g., systemic volume, vascular resistance, heart rate, left ventricular size and contraction (25–28)), allowing for prediction of the level of support and pump stroke volume that would be needed for children with BSAs between 0.6 and 1.5 m^2. Dilated cardiomyopathy was simulated with three patient sizes (0.6, 1.0, and 1.5 m^2) and hemodynamics were assessed for synchronous counterpulse support for stroke volumes from

Author Manuscript Author Manuscript Author Manuscript Author Manuscript

5 to 30 ml. From this analysis, it was determined that a TORVAD with 15 ml stroke volume in counterpulse would be sufficient to provide adequate support for the majority of patients in the target size range. By operating in synchronous counterpulse support, the TORVAD preserves the majority of native aortic valve flow and increases cardiac output with a single synchronous counterpulse in early diastole. Figure 3 shows a typical healthy cardiac output (28) and the results from the simulation - namely, cardiac output in heart failure, and cardiac output with 15 ml counterpulse TORVAD support.

Due to patient variation in HF condition and severity, a 15 ml stroke volume may not be ideal for all patients in the target range and some patients might need more or less flow. Therefore, the pump can also operate asynchronously up to 4 L/min, which is sufficient to provide a normal healthy cardiac output for a child with a BSA of 1.5 m^2. Additionally, the TORVAD platform technology could be scaled to various sizes such as 5, 10, 15, 20, and 30 ml to provide patient-targeted support similar to the various sizes of the Berlin Heart EXCOR® extracorporeal VAD (29).

Magnetic Coupling Model

The magnetic linkage enables individual position control of the pistons as they move within the toroidal pump chamber through a magnetic coupling to the position-controlled motors outside the pump chamber. The adult version of the TORVAD relies on C-shaped magnetic linkages with 5-magnet Halbach arrays (30) to maximize the flux density in the air gap while providing low-angle offset coupling between the motor and piston positions. By having magnetic couplings on opposite sides of the piston, axial forces from each of the magnetic couplings offset one another, thereby reducing the load on the microhydrodynamic ceramic bearings.

With the goal of miniaturization for the pediatric TORVAD, the design for the magnetic coupling has been changed from the C-shape design where the magnetic coupling is through both the top and bottom of the torus to a radial coupling where the magnetic coupling is through the inner radial wall of the torus. This change eliminates the empty volume above and below the torus within which the C-shaped magnets rotated which 1) decreases the magnetic linkage volume by 65%, thereby reducing overall pump volume and 2) facilitates a more direct heat transfer pathway from the motors to the thermally-efficient blood-contacting surfaces of the device. Figure 4 shows cross-section schematics of the C-shaped coupling of the adult TORVAD compared to the inner-radial coupling of the pediatric TORVAD. The challenge with this radial coupling design is in achieving a magnetic radial normal force that will minimize the load on the microhydrodynamic bearings while maintaining strong angular coupling between the motor and piston. The design goals for the magnetic coupling were defined as 1) magnetically couple through the inner radial face of the piston only, 2) maintain magnetic coupling up to at least a 300 mmHg pressure across the piston, and 3) minimize the normal radial force on the ceramic bearings.

The radial magnetic coupling consists of an assembly of two 5-magnet Halbach arrays that provide low-angle offset coupling between the motor and piston and one large repulsion magnet to counteract the radial force generated by the Halbach arrays. Three-dimensional FEMs are used to predict the forces from the magnetic coupling. Magnet geometries such as

Author Manuscript Author Manuscript Author Manuscript Author Manuscript

angular width, motor magnet thickness, piston magnet thickness, the Halbach-to-repulsion magnet volumetric ratio, and the air gap were optimized using parametric analysis. Rare earth neodymium iron boron N45SH magnetic properties for residual induction and coercivity properties are assigned for the magnets, and an auto-adaptive tetrahedral mesh is employed for finite element modeling. Force and torque are computed for the piston and rotor magnet subassembly with the magnetostatic field simulator. In-house testing has been used verify the material properties so that these design analysis predictions can be used with reasonable confidence. This can be critical given variability particularly with commercially available yet custom-sized magnets.

The magnetic assembly is simulated with angular displacement between the rotor and piston magnets from zero to 7 degrees. Radial and tangential force on the piston magnets and torque on the rotor magnets are determined by the computational method of virtual work. Tangential force on the piston is converted to a differential pressure across the piston by dividing by the piston area, providing a relationship between pressure and motor torque needed to design the motor. The results from this analysis are plotted in Figure 5. The magnetic assembly has strong angular coupling, ensuring magnetic coupling to pressures exceeding 300 mmHg while keeping normal radial forces below 2.5N.

Motor Model

Pediatric motor design requirements are determined by the operating torque and allowable power. Dynamic torque requirements are calculated from the cardiovascular system model and the pressure/torque relationship obtained from the magnetic simulation. For robust design, the motor power and torque is determined under the maximum design flow rate of 4 L/min. An example of the torque required for each motor resulting from this analysis is plotted in Figure 6(a).

Magnetostatic FEMs are used to optimize motor performance. Motor geometries such as optimal tooth width, tooth length, rotor magnetic thickness, coil wire diameter, and slot-to-pole ratios were optimized using parametric analysis. The motors are optimized for efficiency and minimal torque ripple. An 18 slot, 20 magnet motor was found to provide the best motor characteristics. An example of the FEM results can be seen in Figure 6(b). The small size and efficiency requirements make machine winding of motors increasingly difficult due to the required clearances. Instead, manufacturability is improved by adopting pre-wound coils that can be assembled onto straight-tooth motor stators. A drawing illustrating this design can be seen in Figure 6(c).

Dynamic torque requirements from the cardiovascular model and results of the motor model analysis estimate that each motor will dissipate about 1.9 Watts of electrical power during maximum flow rate support of 4 L/min.

Heat Transfer and Thermal Design

Heat generated by the motors flows to the surrounding tissue and into the blood in the toroidal pumping chamber. The temperature on the surfaces of the device must remain below threshold levels that could cause damage to contacting tissue (41°C), necrosis (42°C), or protein denaturation (40°C) (31–34). International guidelines for implantable medical

Author Manuscript Author Manuscript Author Manuscript Author Manuscript

devices recommend that device surface temperatures not exceed 39°C, or 2°C above the surrounding body temperature of 37°C (35). This criterion has been adopted for this design. It is important to recognize how critical it is to manage the thermal design of any VAD during a miniaturization design process. In particular, the heat generated by the motors needs to be effectively removed, and this makes it necessary to have a detailed accounting of the material and geometric properties of the VAD components since these form the pathways through which heat will flow.

There are two primary pathways for heat to flow: 1) into blood passing through the pumping chamber and 2) into tissue surrounding the device. Heat flow into the surrounding tissue is primarily through capillary perfusion (36) and can be represented using a convection coefficient at the boundary. In this study by Davies et al, heating devices with temperature sensors were implanted in calves adjacent to lung and muscle tissue for a period of 7 weeks. At 0.04 W/cm^2 heat flux density the temperature rise next to the surrounding muscle was 1.6°C, yielding an equivalent convection coefficient of 250 W/m^{2}K.

To determine the convection coefficient for the blood contacting surfaces of the pump (h_b), the flow characteristics and profiles must be assessed (37). Blood flow in the torus chamber is treated as flow through a non-circular tube, which has well defined analytical solutions for flow and experimentally derived approximations for convection coefficients. Flow rates of 1.5 and 4 L/min are assessed corresponding to the synchronous and maximum flows. Averaged flows are used for the steady-state thermal model. For these calculations, blood can be assumed to be Newtonian with a viscosity of 0.0035 Pa s, density of 1050 kg/m^3, specific heat of 3.65 kJ/kgK, convection coefficient (k) of 0.5 W/mK, and Prandtl number (Pr) of 25.6. The area of the rectangular torus cross-section is 138 mm^2 and the hydraulic diameter (D) is 13.5 mm. The Reynolds number (Re_D) varies from 650 to 1900 for flow rates from 1.5 to 4.0 L/min, so laminar flow is assumed. To determine the convection coefficient, the Sieder-Tate (38) correlation is used:

$$h_b = \frac{1.86k}{D}\left(\frac{Re_D PrD}{L}\right)^{\frac{1}{3}}$$

The convection coefficient of the blood interface in the flow chamber varies from 800 to 1150 W/m^{2}K for flow rates from 1.5 to 4.0 L/min. This is over three times higher than the convection to the surrounding tissue, providing a design principle for the device to direct as much heat flux to the blood as possible.

Solid models of the heat transfer components of the device (the stator yoke, shell, and torus, and zirconia rail) were imported into a finite-element program for analysis. Blood and tissue contacting components are made from Titanium (Ti6Al4V) with a thermal conductivity of 7.0 W/mK. The ceramic rail that facilitates microhydrodynamic lubrication is zirconia with a thermal conductivity of 2 W/mK. To deliver heat from the center of the device toward the outer radius, it is desirable to use a material with superior structural and thermal properties; therefore the motor stator yoke is made of Aluminum 6061, which has a thermal conductivity of 167 W/mK. Meshing is performed with self-adaptive patch-conforming

Author Manuscript Author Manuscript Author Manuscript Author Manuscript

tetrahedrons. The convection coefficients determined above are assigned to the appropriate surfaces. The pump is symmetric with one motor on each side, so only one-half of the pump is modeled and an insulated boundary condition is assigned where the two halves meet. To model the heat generated by the motor, volumetric heating is applied to a steel cylinder on the stator yoke where the stator laminations are bonded. Parametric analysis was performed on pump geometries such as the aluminum yoke thickness, the insulating air gap size, and the titanium shell thickness to increase heat transfer pathways to the blood and to balance tissue and blood surface temperatures. Two dissipated power conditions determined by the motor model are simulated: nominal synchronous operation (0.9 W dissipative power at 1.5 L/min) and the full-support worst-case condition (1.9 W at 4 L/min), which reach temperatures of 0.5 and 0.9°C above body temperature, respectively, but is well below the 2°C limit. Surface temperature results from the simulation under the worst-case condition are shown in Figure 7.

Other Size Reductions

Further reductions in size can be accomplished by redesigning pump electronics, replacing the ECG sensing lead with pump surface electrodes, and reducing the size of external structural components. For example, electric components can be readily replaced using similar devices available in smaller packages. An epicardial sensing lead has been used to detect cardiac rhythm in the adult TORVAD, and this can be replaced with two leadless ECG electrodes on the surface of the device (as seen in Figure 8), using principles similar to implantable cardiac monitors (39, 40). This change simplifies the design, reduces the size by eliminating the IS-1 receptacle on the pump housing, and eliminates a surgical implantation step. Signal strength is estimated to be approximately 1 mV depending on the orientation of the pump in the chest cavity. While use of the epicardial lead has been demonstrated in both acute and chronic testing of an adult TORVAD, efficacy of the surface electrodes on the VAD housing will need to be similarly evaluated.

Reduction in size of external pump structural components is made in the final stages and structural integrity is verified using structural FEM analysis.

First Version of Pediatric Design

Following an iterative design process, the pediatric TORVAD was designed with a stroke volume of 15 ml and maximum flow rate of 4 L/min. Computational models were used to scale key components of the system: the magnetic linkage, the motors, and the pump housing. By following a system wide optimization as described, the size of the device has been reduced by 30% relative to what would have resulted from scaling the adult TORVAD with the C-shaped magnetic linkage coupling. This reduction, as well as the relative size of the key components of the system, is shown in Figure 9.

Conclusion

There is a need for pediatric VADs with reduced adverse event rates. The TORVAD has potential for improved clinical outcomes particularly due to its well-defined low-shear design that is readily scaled to maintain favorable hematological characteristics. A design

Author Manuscript Author Manuscript Author Manuscript Author Manuscript

process has been described and used to scale the TORVAD for pediatric patients with a BSA between 0.6 and 1.5 m^2 using an iterative optimization approach. Results of this work for the pediatric pump include optimizations that can be applied to reduce the size and improve efficiency of the adult TORVAD. The process includes detailed methods for redesigning the magnetic coupling linkage, the integrated motors, and for achieving an effective thermal design. This iterative design approach can be used to design and develop a TORVAD platform technology consisting of several devices with stroke volumes ranging from 5 to 30 ml. These devices will be able to meet a broad range of patient needs while maintaining a highly favorable hematological performance profile

Acknowledgments

This research was supported by the National Heart, Lung, and Blood Institute of the National Institutes of Health under Award Numbers R44HL127833 and R44HL117446. The content is solely the responsibility of the authors and does not necessarily represent the official views of the National Institutes of Health.

References

1. Rossano JW, Kim JJ, Decker JA, et al. Prevalence, morbidity, and mortality of heart failure-related hospitalizations in children in the United States: a population-based study. J Card Fail. 2012; 18:459–70. [PubMed: 22633303]
2. Mansfield RT, Lin KY, Zaoutis T, et al. The Use of Pediatric Ventricular Assist Devices in Children's Hospitals From 2000 to 2010: Morbidity, Mortality, and Hospital Charges. Pediatr Crit Care Med. 2015; 16:522–8. [PubMed: 25850863]
3. Colvin-Adams M, Smithy JM, Heubner BM, et al. OPTN/SRTR 2012 Annual Data Report: heart. Am J Transplant. 2014; 14(Suppl 1):113–38. [PubMed: 24373170]
4. Jefferies JL, Morales DL. Mechanical circulatory support in children: bridge to transplant versus recovery. Curr Heart Fail Rep. 2012; 9:236–43. [PubMed: 22805892]
5. Rossano JW, Lorts A, VanderPluym CJ, et al. Outcomes of pediatric patients supported with continuous-flow ventricular assist devices: A report from the Pediatric Interagency Registry for Mechanical Circulatory Support (PediMACS). J Heart Lung Transplant. 2016; 35:585–90. [PubMed: 27056612]
6. Meyer AL, Malehsa D, Budde U, Bara C, Haverich A, Strueber M. Acquired von Willebrand syndrome in patients with a centrifugal or axial continuous flow left ventricular assist device. JACC Heart Fail. 2014; 2:141–5. [PubMed: 24720921]
7. Chiu WC, Girdhar G, Xenos M, et al. Thromboresistance comparison of the HeartMate II ventricular assist device with the device thrombogenicity emulation-optimized HeartAssist 5 VAD. J Biomech Eng. 2014; 136:021014. [PubMed: 24337144]
8. Mokadam NA, Andrus S, Ungerleider A. Thrombus formation in a HeartMate II. Eur J Cardiothorac Surg. 2011; 39:414. [PubMed: 20656499]
9. Snyder TA, Watach MJ, Litwak KN, Wagner WR. Platelet activation, aggregation, and life span in calves implanted with axial flow ventricular assist devices. Ann Thorac Surg. 2002; 73:1933–8. [PubMed: 12078793]
10. Pappalardo F, Scandroglio AM, Potapov E, et al. Argatroban anticoagulation for heparin induced thrombocytopenia in patients with ventricular assist devices. Minerva Anestesiol. 2012; 78:330–5. [PubMed: 22357371]
11. Geisen U, Heilmann C, Beyersdorf F, et al. Non-surgical bleeding in patients with ventricular assist devices could be explained by acquired von Willebrand disease. Eur J Cardiothorac Surg. 2008; 33:679–84. [PubMed: 18282712]
12. Meyer AL, Malehsa D, Bara C, et al. Acquired von Willebrand syndrome in patients with an axial flow left ventricular assist device. Circ Heart Fail. 2010; 3:675–81. [PubMed: 20739614]

Author Manuscript Author Manuscript Author Manuscript Author Manuscript

13. Lewis, CS., Houzelle, A., Snyder, TA., Schmidtke, DW. Effect of High Shear Exposure on Neutrophil Rolling Behavior. ASAIO Conference; June 19, 2014; Washington, DC. 2014.
14. Carter J, Hristova K, Harasaki H, Smith WA. Short exposure time sensitivity of white cells to shear stress. ASAIO J. 2003; 49:687–91. [PubMed: 14655735]
15. Larson, ER., Gohean, JR., Longoria, RG., Smalling, RW., Kurusz, M. Low-shear TORVAD Ventricular Assist Device Preserves von Willebrand Factor in Chronic Ovine Model. 61st Annual Conference of the American Society for Artificial Internal Organs; June 24–27; Chicago, IL. 2015.
16. Gohean, JR., Larson, ER., Longoria, RG., Smalling, RW., Kurusz, M. Preservation of High Molecular Weight vWF and Low Hemolysis With the Low Shear TORVAD Ventricular Assist Device. 61st Annual Conference of the American Society for Artificial Internal Organs; June 24–27; Chicago, IL. 2015.
17. Rosenthal DN, Almond CS, Jaquiss RD, et al. Adverse events in children implanted with ventricular assist devices in the United States: Data from the Pediatric Interagency Registry for Mechanical Circulatory Support (PediMACS). J Heart Lung Transplant. 2016; 35:569–77. [PubMed: 27197775]
18. Gohean JR, George MJ, Chang KW, et al. Preservation of native aortic valve flow and full hemodynamic support with the TORVAD using a computational model of the cardiovascular system. ASAIO J. 2015; 61:259–65. [PubMed: 25485562]
19. Longoria, RG., Gohean, JR., Larson, ER., Smalling, RW., Kurusz, M. Direct measurement of the LV-aortic differential pressure using the TORVAD left-ventricular assist device. 61st Annual Conference of the American Society for Artificial Internal Organs; June 24–27; Chicago, IL. 2015.
20. Panton, RL. Incompressible Flow. Wiley; 1996.
21. Thamsen B, Mevert R, Lommel M, et al. A two-stage rotary blood pump design with potentially lower blood trauma: a computational study. Int J Artif Organs. 2016; 39:178–83. [PubMed: 27034319]
22. Thamsen B, Blumel B, Schaller J, et al. Numerical Analysis of Blood Damage Potential of the HeartMate II and HeartWare HVAD Rotary Blood Pumps. Artif Organs. 2015; 39:651–9. [PubMed: 26234447]
23. Gohean JR, George MJ, Pate TD, Kurusz M, Longoria RG, Smalling RW. Verification of a computational cardiovascular system model comparing the hemodynamics of a continuous flow to a synchronous valveless pulsatile flow left ventricular assist device. ASAIO J. 2013; 59:107–16. [PubMed: 23438771]
24. Gohean, JR., Pate, TD., Longoria, RG., Smalling, RW., Kurusz, M. Comparison of a Valveless Pulsatile Assist Device with Continuous Flow in a Computational Model of the Cardiovascular System. 57th Annual Conference of the American Society for Artificial Internal Organs; June 10–12; Washington, DC. 2011.
25. Giridharan GA, Koenig SC, Mitchell M, Gartner M, Pantalos GM. A computer model of the pediatric circulatory system for testing pediatric assist devices. ASAIO J. 2007; 53:74–81. [PubMed: 17237652]
26. Goodwin JA, van Meurs WL, Sa Couto CD, Beneken JE, Graves SA. A model for educational simulation of infant cardiovascular physiology. Anesth Analg. 2004; 99:1655–64. table of contents. [PubMed: 15562049]
27. Sharp MK, Pantalos GM, Minich L, Tani LY, McGough EC, Hawkins JA. Aortic input impedance in infants and children. J Appl Physiol (1985). 2000; 88:2227–39. [PubMed: 10846040]
28. de Simone G, Devereux RB, Daniels SR, et al. Stroke volume and cardiac output in normotensive children and adults. Assessment of relations with body size and impact of overweight. Circulation. 1997; 95:1837–43. [PubMed: 9107171]
29. Miera O, Schmitt KR, Delmo-Walter E, Ovroutski S, Hetzer R, Berger F. Pump size of Berlin Heart EXCOR pediatric device influences clinical outcome in children. J Heart Lung Transplant. 2014; 33:816–21. [PubMed: 24836553]
30. Halbach K. Design of permanent multipole magnets with oriented rare earth cobalt material. Nuclear Instruments and Methods. 1980; 169:1–10.

Author Manuscript Author Manuscript Author Manuscript Author Manuscript

31. Pasha R, Benavides M, Kottke-Marchant K, Harasaki H. Reduced expression of platelet surface glycoprotein receptor IIb/IIIa at hyperthermic temperatures. Lab Invest. 1995; 73:403–8. [PubMed: 7564273]
32. Hershkoviz R, Alon R, Mekori YA, et al. Heat-stressed CD4+ T lymphocytes: differential modulations of adhesiveness to extracellular matrix glycoproteins, proliferative responses and tumour necrosis factor-alpha secretion. Immunology. 1993; 79:241–7. [PubMed: 8102119]
33. Seese TM, Harasaki H, Saidel GM, Davies CR. Characterization of tissue morphology, angiogenesis, and temperature in the adaptive response of muscle tissue to chronic heating. Lab Invest. 1998; 78:1553–62. [PubMed: 9881955]
34. Yamazaki K, Litwak P, Kormos RL, et al. An implantable centrifugal blood pump for long term circulatory support. ASAIO J. 1997; 43:M686–91. [PubMed: 9360134]
35. Standardization IOf. Implants for surgery - Active implantable medical devices - Part 1: General requirements for safety, marking and for information to be provided by the manufacturer. ISO; 2000. ISO 14708-1.
36. Davies CR, Fukumura F, Fukamachi K, et al. Adaptation of tissue to a chronic heat load. ASAIO J. 1994; 40:M514–7. [PubMed: 8555569]
37. Gardiner JM, Wu J, Noh MD, et al. Thermal Analysis of the PediaFlow pediatric ventricular assist device. ASAIO J. 2007; 53:65–73. [PubMed: 17237651]
38. Sieder EN, Tate GE. Heat Transfer and Pressure Drop of Liquids in Tubes. Ind Eng Chem. 1936; 28:1429–35.
39. Tomson TT, Passman R. The Reveal LINQ insertable cardiac monitor. Expert Rev Med Devices. 2015; 12:7–18. [PubMed: 25154970]
40. Hindricks G, Pokushalov E, Urban L, et al. Performance of a new leadless implantable cardiac monitor in detecting and quantifying atrial fibrillation: Results of the XPECT trial. Circ Arrhythm Electrophysiol. 2010; 3:141–7. [PubMed: 20160169]

Author Manuscript Author Manuscript Author Manuscript Author Manuscript

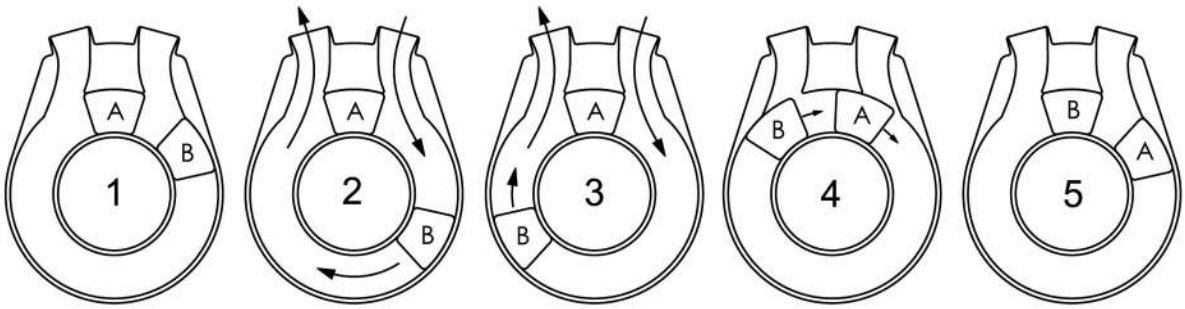

Figure 1.

A schematic representation of the TORVAD with two independently controlled pistons, A and B, within a toroidal chamber. Pumping is achieved by driving one piston around the chamber while holding the position of the other piston between the inlet and outlet ports to serve as a "virtual" valve. From rest (1), the drive piston (B) begins to rotate (2), whereas the valve piston (A) facilities unidirectional flow. Piston (B) begins to decelerate (3) as it nears completion of a stroke, at which time both pistons move together (4) and then momentarily come to rest (5). At this point, the roles of the pistons have been reversed; on the next stroke (A) will act as the drive piston and (B) as the valve piston.

Author Manuscript Author Manuscript Author Manuscript Author Manuscript

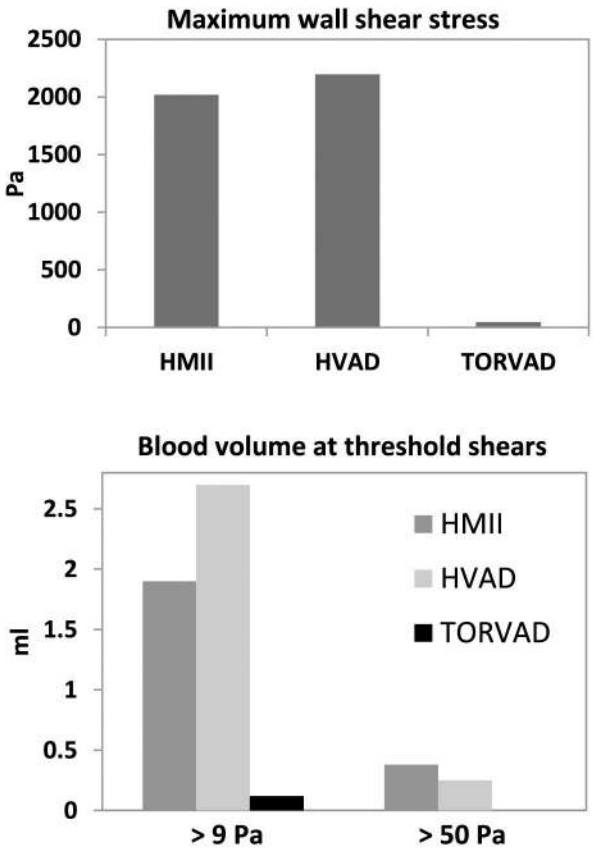

Figure 2.

Maximum wall shear stress in the TORVAD and two continuous flow devices, the Thoratec HeartMate II® (HMII) and the HeartWare HVAD®, and blood volume estimated to exceed approximate thresholds for vWF unfolding (9 Pa) and platelet activation (50 Pa). The TORVAD has maximum wall shear stress two orders of magnitude less than continuous flow devices and only a small volume fraction of blood is exposed to shear above 9 Pa. No volume of blood in the TORVAD is exposed to shear above 50 Pa. Values for continuous flow devices were estimated using computational fluid dynamics as described by Thamsen et al (21, 22).

Author Manuscript Author Manuscript Author Manuscript Author Manuscript

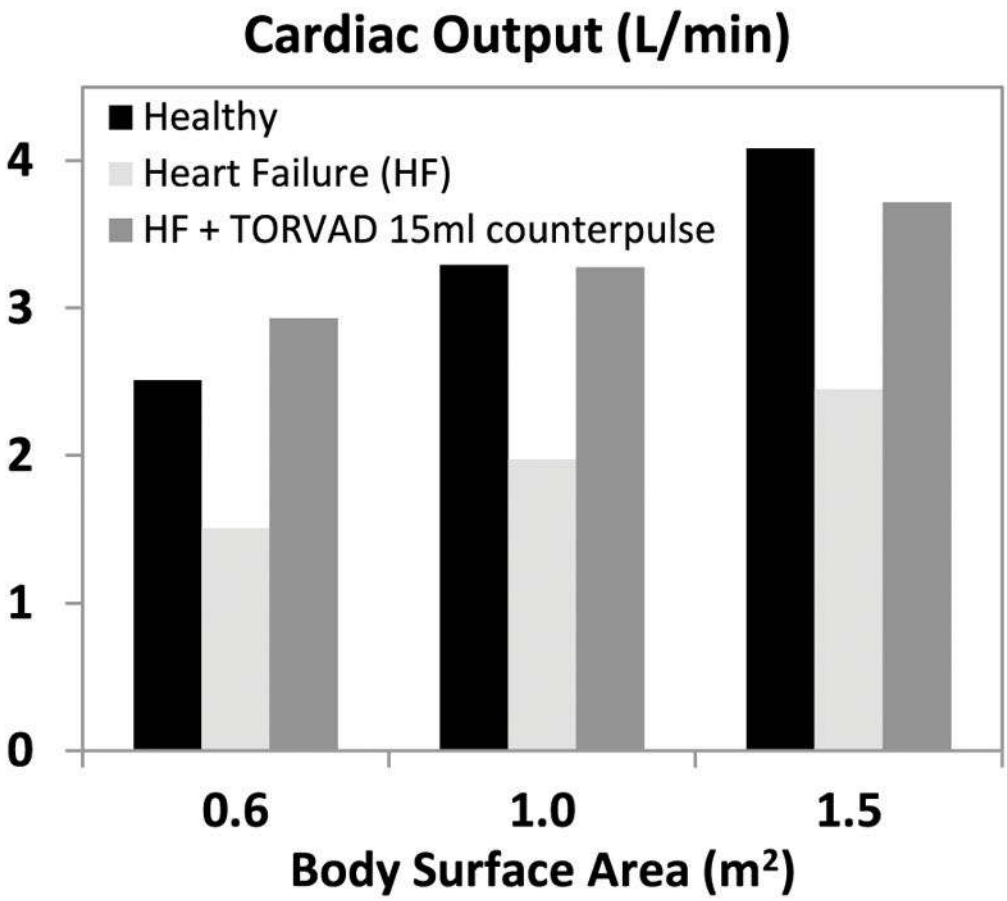

Figure 3.
Computational simulation predictions of cardiac output for healthy cardiac function, heart failure, and heart failure with 15 ml counterpulse TORVAD support for three representative body surface areas (BSAs) in the targeted patient range (0.6 to 1.5 m^2).

Author Manuscript Author Manuscript Author Manuscript Author Manuscript

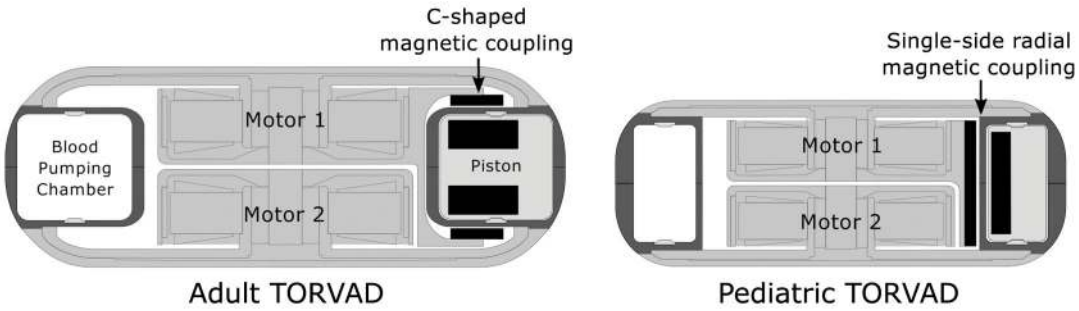

Figure 4.

Cross-sections of the adult and pediatric TORVADs illustrating the location of the motors in the pump and how they are magnetically coupled to the pistons. In this case, motor 1 is shown coupled to a piston, but the piston and magnetic coupling are not shown for motor 2.

Author Manuscript Author Manuscript Author Manuscript Author Manuscript

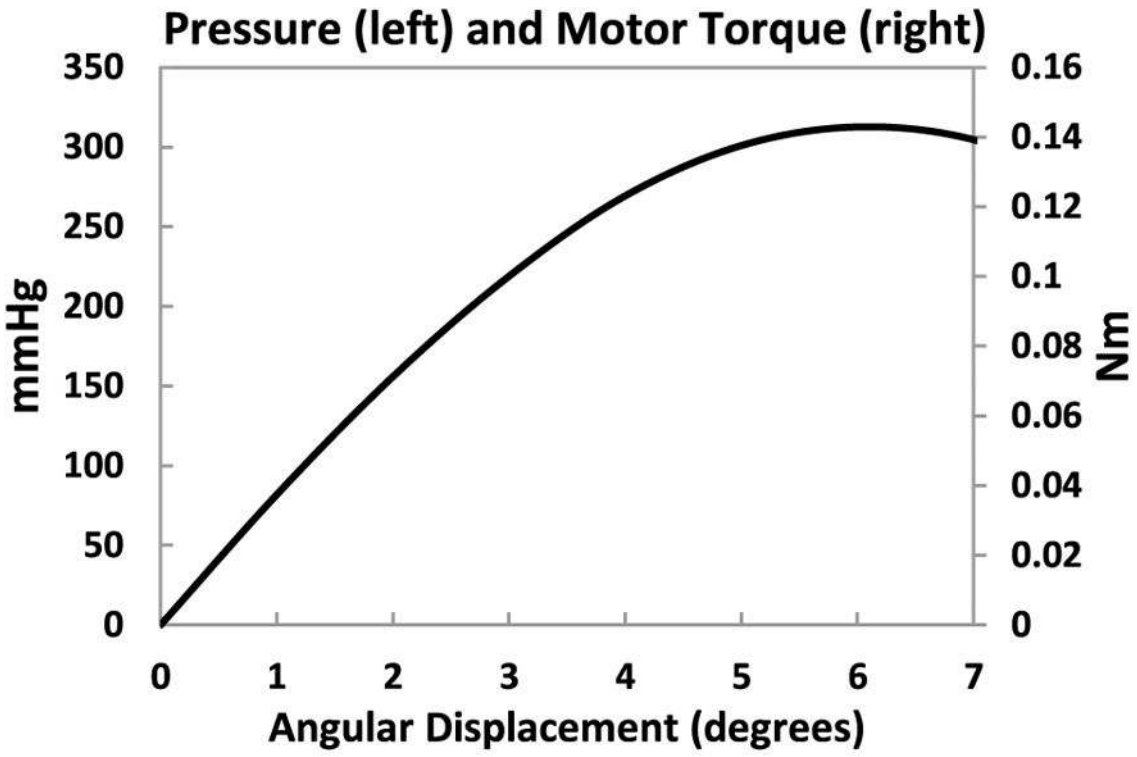

Figure 5.

Results from a three-dimensional finite element model of the radial magnetic coupling: the differential pressure across a piston and the torque on the rotor magnets vs the angular displacement between the rotor and piston magnets. This result provides the relationship between pressure and torque needed for the motors and confirms that the design exceeds the goal of 300 mmHg maximum pressure.

Author Manuscript Author Manuscript Author Manuscript Author Manuscript

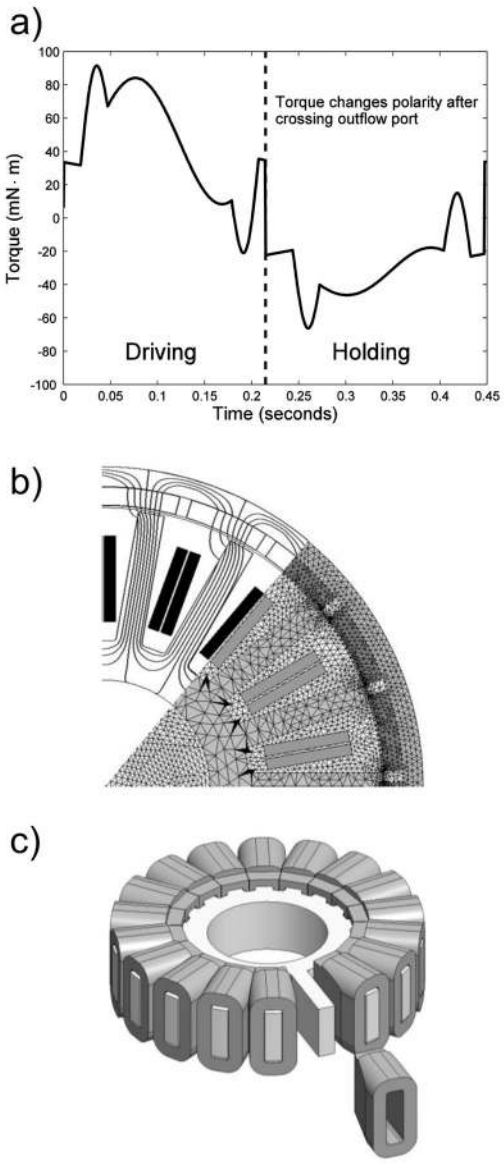

Figure 6.

a) Example of required motor torque for pump loading conditions at 4 L/min flow against a mean differential pressure of 70 mmHg. Motor torque reflects contributions from: blood pressure in the systemic circulation and left ventricle, resistive and inertia of the fluid in the inflow and outflow cannulas and torus, inertial force of the piston mass, inertial torque of the motors, and damping from the hydrodynamic bearings. b) Motor model showing magnetic flux lines and mesh used in finite-element analysis. c) Motor armature showing preformed coils that slide into place to aid assembly.

Author Manuscript Author Manuscript Author Manuscript Author Manuscript

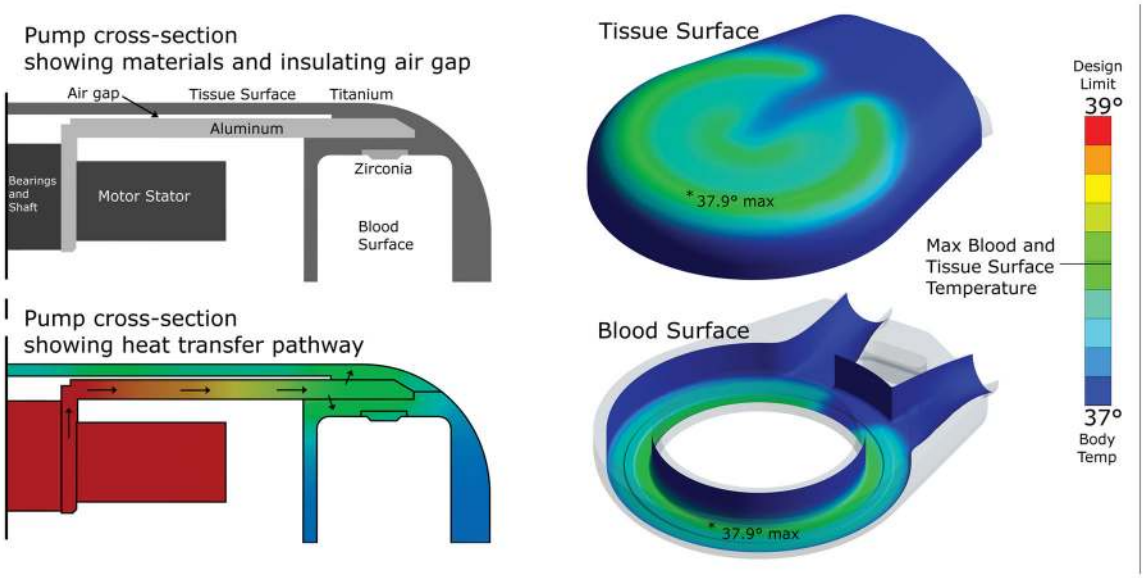

Figure 7.

Surface temperatures on the tissue and blood interfacing surfaces during worst-case full support dissipative power conditions at 4 L/min pump flow. 37°C is the body temperature and 39°C is the design limit. Both surfaces reach maximum temperatures of 37.9°, only 0.9° above ambient and well below the design limit, thereby providing a substantial safety factor.

Author Manuscript Author Manuscript Author Manuscript Author Manuscript

Figure 8.
Rendered image of the adult (left) and pediatric (right) TORVAD.

Author Manuscript Author Manuscript Author Manuscript Author Manuscript

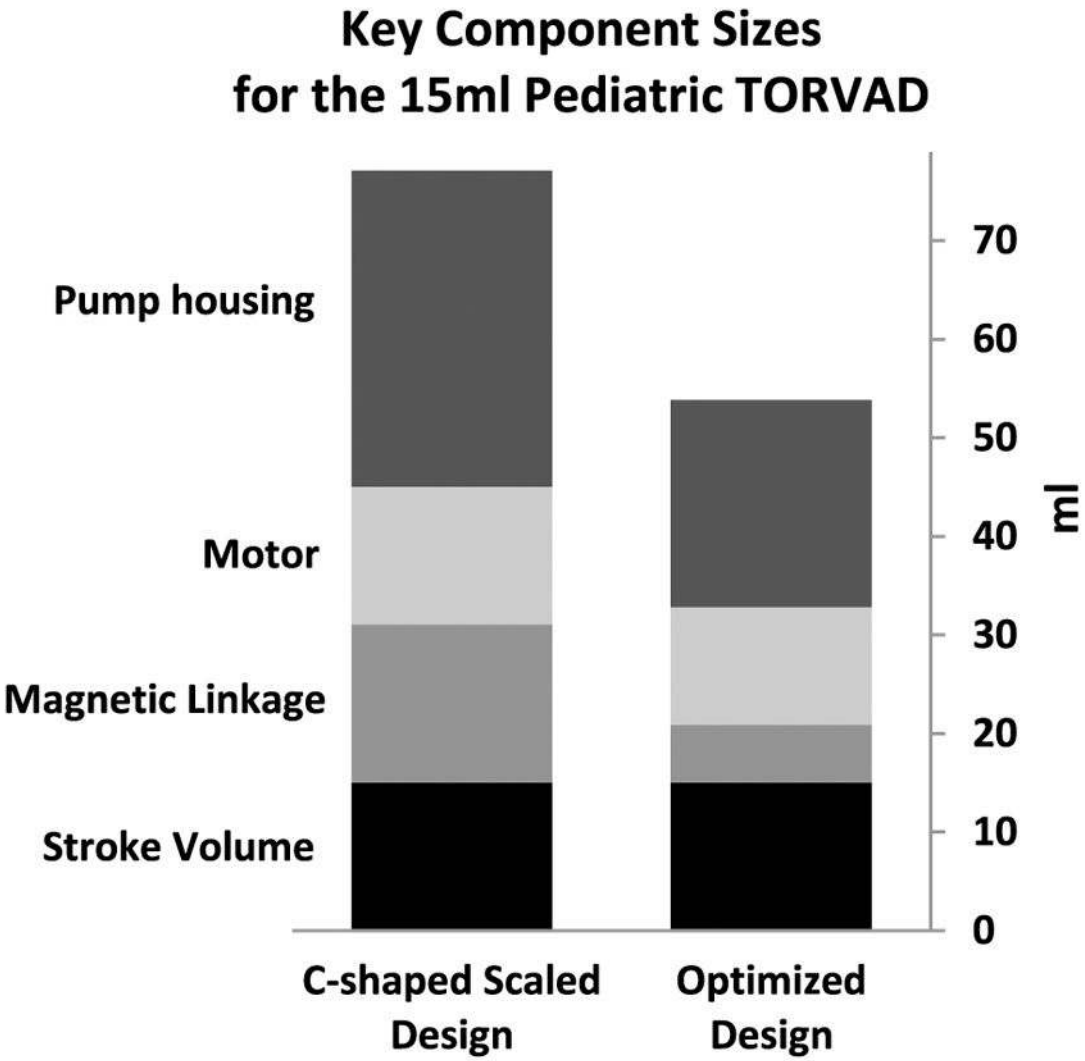

Figure 9.

Size reduction resulting from iterative optimization design. Stroke volume is fixed for the device and cannot be reduced, but the key pump components, the pump housing, motor, and magnetic linkage, were each made significantly smaller than a geometric scaling of the adult device with the C-shaped magnetic linkage coupling.